https://doi.org/10.32604/zkg.2026.077166

ARTICLE

Effect of cement content on the performance of static cracking agent

Jingshu Shao[1], Peiyuan Chen[1,2,3,*], Yankun Ma[2,3,4], Aiguo Wang[5,*], Weibo Tan[1] and Dingzou Tang[2,3,4]
[1]School of Civil Engineering and Architecture, Anhui University of Science and Technology, Huainan, China
[2]National Key Laboratory of Deep Coal Safe Mining and Environmental Protection, Anhui University of Science and Technology, Huainan, China
[3]Key Laboratory of Safe and Effective Coal Mining Ministry of Education, Anhui University of Science and Technology, Huainan, China
[4]Scientific Research and Development Platform of Technology of Disaster Prevention in Deep Coal Mines, Anhui University of Science and Technology, Huainan, China
[5]Anhui Province Engineering Laboratory of Advanced Building Materials, Anhui Jianzhu University, Hefei, China
*Corresponding Authors: Peiyuan Chen. Email: peiyuan29@126.com; Aiguo Wang. Email: wag3134@126.com

Received: 03 December 2025; Accepted: 10 July 2026

ABSTRACT: Conventional blasting for rock and concrete demolition in sensitive environments inevitably generates adverse effects such as excessive noise, vibration, and flying rocks. To avoid these problems, static cracking agents (SCAs) provide a safer and more practical alternative by fracturing rock or concrete through the substantial volumetric expansion associated with the hydration of CaO to $Ca(OH)_2$. However, conventional SCA suffers from inherent drawbacks, including relatively rapid hydration reaction rates and unstable expansion performance. To address these limitations, this study focuses on regulating the hydration reaction process and expansion performance of SCA by adjusting the proportion of cementitious materials in their composition. The experimental results show that a cement content of 12% provides the optimal expansion performance, with a volumetric expansion ratio of approximately 600%. Meanwhile, the hydration reaction is effectively moderated, and the peak temperature occurs at approximately 15 min. The mixture containing 10% cement exhibited the earliest crack initiation and the highest average crack-width development rate of 4.50 mm/min, whereas the mixture containing 12% cement achieved the highest volumetric expansion ratio and an average crack-width development rate of 2.35 mm/min. In summary, compared with conventional SCAs, adjusting the proportion of cementitious materials enables effective control over the hydration reaction rate and expansion performance of SCAs. This research provides valuable theoretical support for the design and application of high-performance SCA in rock and concrete demolition under complex engineering conditions.

KEYWORDS: Static cracking agent; hydration reaction regulation; expansion performance; cement content effect; concrete cracking behavior

MATERIALS

1 Introduction

In recent decades, static cracking agent (SCA) has emerged as a greener and safer alternative to explosive blasting methods for demolitions of rock and concrete in engineering fields, owing to its advantages of low noise, minimal vibration, and absence of fly rock [1, 2]. This method is particularly valuable when rock or concrete must be demolished in densely populated or environmentally sensitive areas since conventional blasting, while efficient, often leads to excessive noise, vibration, and fly rock, posing severe safety and environmental risks [3, 4].

Mechanistically, CaO is generally the principal reactive component of SCA, and the hydration of CaO can produce immense expansive pressure to internally fracture surrounding rock or concrete [5]. Existing studies revealed that the composition and the hydration environment are the two crucial factors in influencing the breaking efficiency of SCA. It has been reported by Li et al. [6] that the optimal CaO content was approximately 70%, producing an expansion pressure 25–30% higher than that of the other mixtures in their orthogonal experiments. Li et al. [7] found that in addition to CaO, the cementitious components also play an important role. Experimental results showed that when the water–binder ratio was decreased from 0.35 to 0.25, the peak expansive pressure of SCA increased from about 28 MPa to nearly 36 MPa. In addition, other admixtures can also affect the efficiency of SCA. For instance, Maneenoi et al. [8] reported that adding 2% $CaCl_2$ as an accelerator increased the early expansive pressure of SCA by approximately 40% within the first 6 h. Natanzi et al. [9] reported that the reaction rate decreased by up to 64% at an ambient temperature of 2°C, indicating that higher temperatures are more favorable for SCA hydration.

Liu et al. [1] further proposed a hydration accelerating method for SCA through microwave. It showed that the application of microwave can greatly speed up the hydration of CaO to produce stronger expansion stress and improved breaking efficiency.

Among all the components of SCA, cement plays a critical role in influencing the performance of SCA, in addition to CaO. It has been revealed that the hydrated cement can provide a stable and uniform stress-transmitter with suitable strengths [10, 11]. In addition, the presence of cement can also induce benefits like regulate the hydration reaction rate and control the release rhythm of expansion pressure [2, 10]. One can thus find that the content of cement should be a critical factor to adjust the performance of SCA, considering that a low content of cement may fail to generate a good synergistic effect with CaO to well transfer expansion stress, while an excessive content of cement would impede the expansion of CaO, causing internal structural failure of the hydrated SCA matrix [10]. However, although previous studies have examined the effects of CaO content, water–binder ratio, admixtures, and environmental conditions, the systematic role of cement dosage in regulating the coupled hydration–mechanical behavior of CaO-based SCA systems remains insufficiently clarified. In particular, the interaction among water competition, hydration rate modulation, skeleton formation, and expansion stress transmission has not been comprehensively elucidated. A clear mechanistic understanding of this coupled regulation is essential for designing SCAs with controllable reaction kinetics and optimized expansion efficiency.

Accordingly, this study investigates the effects of cement dosage on the fresh properties, reaction rate, expansion pressure, volumetric expansion, hydration products, and microstructure of SCA. The cracking behavior of concrete with SCA is also studied to reveal the mechanism.

2 Materials and methods

2.1 Materials

Ordinary Portland cement (P·O 42.5) with a Brunauer–Emmett–Teller (BET) area of 1652 m^2/kg and an apparent density of 3100 kg/m^3 was purchased from Anhui Conch Cement Co., Ltd. CaO of analytical purity was used as the expansive agent. Analytical reagent grade gypsum with a particle size of 75 µm, together with analytical reagent grade citric acid, were obtained from commercial suppliers in Tianjin, China, and served as additives. Bentonite containing not less than 85% montmorillonite and having a specific surface area of 600 m^2/g, as well as class F fly ash with a particle size of 75 µm, were supplied from Jiangxi and Hebei, China, respectively, and used as water retention agents and fillers. A RHEOPLUS 411 polycarboxylic superplasticizer with a water-reducing rate of 30%–40% was provided by Jiangsu Subo New Materials Co., Ltd. The mixing water was ordinary tap water.

2.2 Mix proportion and sample preparation

Five SCA mixtures were designed, as shown in Table 1. The w/b for all SCAs was 0.3 with a good flowability. The control, named Con, has a cement content accounting for 6% of the total solid mass. The control mixture (Con) was designed based on mixture proportions commonly reported in previous studies on conventional CaO-based static cracking agents, and therefore represents a typical baseline formulation in existing literature [7, 12, 13]. For the other SCA with more cement, cement was added as the substitution of fly ash, named Aac20, Aac40, Aac60, and Aac80. During a typical mixing process, cement, gypsum, bentonite, and fly ash were first mixed using a Harbor mixer. Then, superplasticizer and citric acid were added and mixed for 3 min. In final, CaO was added by stirring 1 min. All mixing procedures were conducted under controlled laboratory conditions (20 ± 2°C; relative humidity 60 ± 5%) to reduce environmental variability.

2.3 Experimental methods

2.3.1 Setting time and fluidity

The initial setting times of SCA were determined using a Vicat needle apparatus under standard environmental conditions [7].

The fluidity of SCA was measured by the mini-slump method. The average spread in two perpendicular directions was recorded [7].

For each mixture, three independent specimens were tested, and the reported values represent the average of parallel measurements.

2.3.2 Reaction rate

The reaction rate of SCA was assessed by monitoring the temperature evolution of a 500 g SCA (w/b = 0.30) placed in a foam insulation box and measured at the center with a HIOKI LR8431-30 data acquisition system. Temperature was recorded

Table 1 Mixing proportions of SCA/kg/m^3

Mixture	CaO	Cement	Gypsum	Bentonite	Fly Ash	Superplasticizer	Citric Acid	Water
Con	1752	144	72	96	264	48	24	698
Aac20	1752	192	72	96	216	48	24	698
Aac40	1752	240	72	96	168	48	24	698
Aac60	1752	288	72	96	120	48	24	698
Aac80	1752	336	72	96	72	48	24	698

every 3 min until stabilization, and the time to peak temperature and maximum temperature rise were taken as indicators of reaction rate and hydration intensity.

Each test was conducted in triplicate to ensure reproducibility, and consistent temperature evolution trends were observed among parallel samples. The presented curves correspond to representative results, while peak values were averaged.

2.3.3 Expansion pressure

According to AQ 1108-2014 [14], customized cold-worked Q235 steel pipes with an outer diameter of 48 mm, an inner diameter of 40 mm, and a total height of 300 mm were adopted, with one end welded to a 4 mm thick steel plate. Strain gauges were arranged at heights of 250 mm (two gauges) and 150 mm (one gauge) from the bottom, and the average readings were used to calculate the radial expansion pressure of the SCA according to the specified formula:

$$P = [\varepsilon_\theta/(2-v)]\left[\left(\frac{r_\theta}{r_i}\right)^2 - 1\right]E$$

$$= [\varepsilon_\theta/(2-v)](K^2-1)E \quad (1)$$

where P denotes the radial expansion pressure produced by SCA, ε_θ denotes the circumferential strain of steel pipe, v denotes the Poisson's ratio of steel pipe, with the value of 0.3, r_θ denotes the outer diameter of steel pipe, r_i denotes the inner diameter of steel pipe, K denotes the diameter coefficient of steel pipe, with the value of r_θ/r_i, E denotes the elasticity coefficient of steel pipe, with the value of 2.06×10^5 MPa.

2.3.4 Volumetric expansion ratio

The prepared samples were placed in a beaker; after the reaction was complete, the samples in the beaker were crushed and compacted to eliminate voids, the volume change was measured, and calculations were performed according to Equation (2) [15].

$$\beta = \frac{Ah}{V_0} \times 100\% \quad (2)$$

where β denotes the volumetric expansion ratio (%), A denotes the bottom area of the vessel, V_0 denotes the volume of the SCA before the reaction, and h denotes the leveling height of the SCA after the reaction.

Three parallel tests were performed for each mixture to ensure measurement stability, and the reported volume expansion ratio represents the average value.

2.3.5 XRD

The hydration products of the SCA were analyzed using a Rigaku SmartLab high resolution X-ray diffractometer with Cu-Kα radiation, tube setting of 40 kV and 30 mA. The scanning rate and scanning range were 2°/min and 2θ = 15°–75°, respectively.

2.3.6 SEM

A Hitachi Flex1000 scanning electron microscope (SEM) was used to examine the surface morphology of the hydrated SCA samples. The observations were conducted in secondary electron (SE) imaging mode to obtain morphological information of hydration products on fractured surfaces. The SEM was operated at an accelerating voltage of 15 kV with a working distance of approximately 10 mm, using a secondary electron detector.

2.3.7 Crack evolution law

A C30 graded concrete was proportioned with a 28-day compressive strength over 30 MPa. Table 2 shows the mixing proportion. The concrete was cast into cubic specimens measuring 150 mm × 150 mm × 150 mm, and PVC pipe was inserted in the middle of specimen to fabricate a hole with a diameter of 40 mm and a depth of 105 mm [7]. The concrete specimen was cured under standard conditions (20 ± 2°C, relative humidity >95%) for 28d. Thereafter, 500 g SCA was mixed and placed in the hole to verify the cracking process of concrete sample.

The crack initiation time (t_i) was defined as the elapsed time from SCA placement to the first visible crack on the concrete surface. The complete failure time (t_f) was defined as the time at which the specimen reached the final recorded cracking state or complete failure. The crack-development duration was calculated as ($\Delta t = t_f - t_i$).

To quantitatively characterize crack-width development after crack initiation, the average crack-width development rate (v_c) was calculated as:

$$v_c = \frac{w_f - w_i}{t_f - t_i} \quad (3)$$

where (w_i) and (w_f) are the crack widths at crack initiation and at the final recorded stage, respectively. For each mixture, the reported values were obtained from three parallel specimens and are expressed as the mean ± standard deviation.

Similarly, the cracking tests were conducted with three parallel specimens for each mixture.

Table 2 Mixing proportion of C30 concrete (kg/m³)

Water	Cement	Fly Ash	Superplasticizer	Sand	Gravel
163	250	63	3.7	729	1189

The presented results correspond to the average performance of repeated tests, and consistent cracking behavior was observed among replicates.

3 Results and discussion

3.1 Fresh properties of SCA

Figure 1 presents the fluidity and initial setting time of SCA with different cement dosages. The fluidity of the fresh SCA mixtures was measured using the mini-slump method in accordance with GB/T 8077-2023 [16]. It shows that all mixtures display a similar fluidity around 23 cm, indicating adequate workability for practical application. As the cement content increased, the fluidity of SCA slightly decreased from 23.0 cm to 22.5 cm, which is probably due to the differences of cement and fly ash in the particle size and shape [17].

A corresponding trend was observed in the initial setting time. As can be seen that increasing the cement content accelerated the setting of SCA as the initial setting time decreased from 24 min to 19 min with increasing cement dosage.

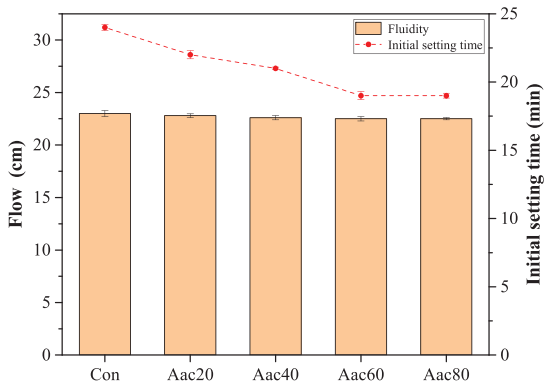

Figure 1 Fluidity and initial setting time of SCA

3.2 Reaction temperature

Figure 2 presents the temperature evolution of the SCA mixtures over a period of 40 min. It shows that the reaction temperature of Con increases rapidly during the initial stage, reflecting the rapid hydration of CaO [18]. By adding more cement, increasing the cement content progressively retarded the temperature rise in SCA mixture, where the increasing rate of reaction temperature tends to decrease with cement content, as typically indicated by the slope of curve during the first minutes. Moreover, the time to reach the peak temperature for each mixture has been delayed associated with cement content, although the mixtures exhibit similar peak temperatures. This trend suggests that cement addition affects the early hydration environment of the CaO-rich SCA system. From a qualitative perspective, this effect may be associated with the competition for available water between CaO hydration and cement hydration. As part of the mixing water is consumed by cement hydration, the rapid heat release caused by CaO hydration may be moderated. In addition, early cement hydration products may partially cover some CaO particles, further slowing the early heat-release process [19–21].

Therefore, when excessive cement has been added, Aac80, the reaction temperature of SCA mixture can be greatly influenced, characterized by a more pronounced retarding effect [22].

3.3 Expansion pressure

Figure 3 presents the expansion-pressure development of the SCA mixtures over 140 min. As can be seen that the expansion pressure of each mixture increases quickly during the first 100 min, thereafter tends to level off over time. Despite of the different values of expansion pressure in each mixture, the turning point, where the expansion pressure starts to level off over time, have been delayed when more cement dosage has been added. This is consistent with the findings from Figure 2, and emphasizes the role of cement in influencing the expansion performance of SCA [23].

The expansion-pressure curves can be divided into three stages: Phase I, Phase II, and Phase III.

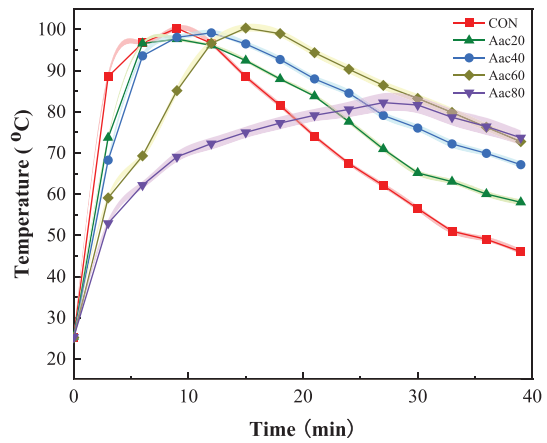

Figure 2 Reaction temperature of SCA

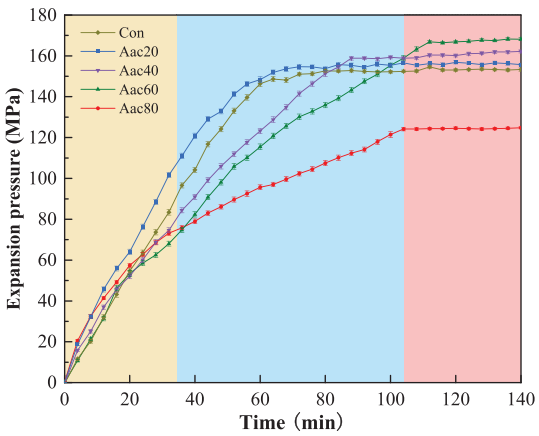

Figure 3 Expansion pressure of SCA

As marked in this figure. During Phase I, the expansion pressures of all SCAs are very close over time. Since CaO hydrates much faster than cement, the similar values of expansion pressure during this phase reveals that CaO hydration may dominate the overall expansion behavior of SCA as all SCA mixtures have the same CaO content. During Phase II, the effect of cement dosage on the expansion pressure of samples becomes more pronounced as the differences in expansion pressure among the mixtures become increasingly pronounced.

It can be found that cement dosage is an important factor in influencing the developing rate of expansion pressure, where a larger cement dosage has induced a slower increase in expansion pressure as indicated by the slope of the ascending part in this phase. This behavior can be qualitatively interpreted as being associated with the gradual formation of cement hydration products within the SCA matrix. These hydration products may improve the continuity of the hydrated matrix and introduce a certain degree of internal confinement, thereby influencing the stress accumulation and transmission process during CaO hydration [19, 20, 24–26]. Under this condition, part of the expansive stress generated by CaO hydration may be consumed in overcoming the internal restraint of the matrix before being effectively transmitted outward, leading to a slower pressure development rate [27–29]. Moreover, the turning point in Phase II is delayed with increasing cement content, suggesting that the stress accumulation process becomes more gradual when the internal confinement of the hydrated matrix increases. For instance, with the addition of 8% to 12% cement, the expansion pressure of SCA increases by approximately 2%–11%. This result indicates that a moderate degree of structural confinement associated with cement hydration may be beneficial for the effective development and transmission of expansion pressure. Nevertheless, the dosage of cement should be optimized as an excessive cement dosage may impose excessive internal constraint that the expansion behavior of SCA is heavily affected. For instance, the expansion pressure of Aac80 is the lowest one within both Phase II and Phase III.

This reduction cannot be simply attributed to delayed hydration. Instead, it may be related to excessive internal confinement within the SCA matrix. With high cement content, the hydrated matrix may become relatively denser, which could restrict the effective conversion of CaO-induced expansion into radial expansion pressure [25, 26, 30, 31]. Under such conditions, part of the expansion effect may be internally constrained within the matrix rather than being fully transmitted to the surrounding steel pipe. Consequently, the measured macroscopic expansion pressure decreases in Aac80.

The SEM observations discussed in Section 3.5 provide auxiliary morphological information that is qualitatively consistent with this interpretation.

3.4 Volumetric expansion ratio

Figure 4 shows the volumetric expansion ratio of SCA, which represents a critical property to crack concrete or rock. It shows that cement dosage is an influencing factor in the expansion behavior of SCA. By increasing cement dosage from 6% to 12%, the expansion ratio of SCA increases significantly. A maximum expansion ratio of as high as around 600% has been gained when the cement content reaches 12%. Further increasing the cement dosage to 14%, the expansion ratio drops to be the smallest one with a value of 400%. Therefore, among the investigated mixtures, a cement content of 12% is optimal specifically for maximizing the volumetric expansion ratio, but it does not necessarily provide the highest concrete cracking efficiency.

The expansion behavior of SCA is mainly governed by CaO hydration and is also influenced by the presence of cement hydration products. The hydration of CaO produces $Ca(OH)_2$, which is the principal source of volumetric expansion in the present CaO-rich system. Meanwhile, cement hydration can generate hydration products such as C–S–H gel, which may improve the continuity of the hydrated matrix and influence stress transmission during expansion [22, 32].

When the cement dosage is within a moderate range, the hydration-product structure formed with cement addition may be beneficial for transferring the expansive stress generated by CaO hydration. This interpretation is consistent with the increase in volumetric expansion ratio from Con to Aac60. However, when the cement content becomes excessive, additional cement hydration may consume more available water and produce a relatively denser matrix, which could restrict the effective expansion of $Ca(OH)_2$ and reduce the macroscopic volumetric expansion ratio [33, 34].

It should be noted that the water-competition and stress-transfer effects discussed here are qualitative explanations based on the observed

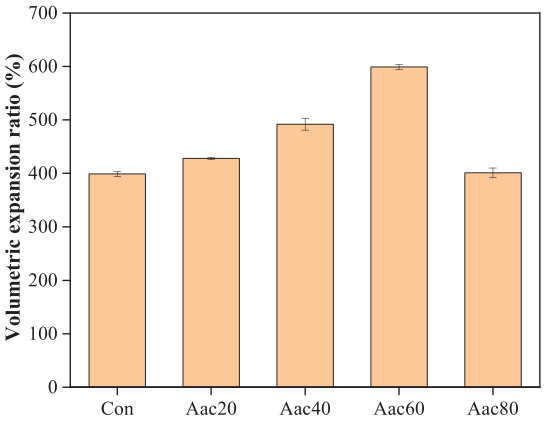

Figure 4 Volumetric expansion ratio of SCA

macroscopic behavior and established hydration theory.

3.5 Composition and microstructure analysis of SCA

3.5.1 XRD

Figure 5 presents the XRD patterns of SCA prepared with different cement dosages. The main crystalline phases identified from the diffraction patterns are $Ca(OH)_2$, calcite, C_2S, C_3S, and CaO, based on the relevant JCPDS reference patterns and literature [1]. In addition, C–S–H is also indicated in Figure 5, as it is one of the principal hydration products formed during cement hydration [35, 36]. Owing to its poorly crystalline or quasi-amorphous nature, C–S–H cannot be accurately identified or quantified as an independent crystalline phase using conventional XRD techniques. Nevertheless, its formation is an inevitable consequence of cement hydration and plays a critical role in the development of the microstructure and mechanical properties of the system [37, 38]. Therefore, the C–S–H label is retained in Figure 5 to indicate the presence of cement hydration products and to facilitate interpretation of the hydration process, rather than to represent a direct quantitative phase identification.

The XRD results show that all SCA samples exhibit highly similar diffraction patterns, with no obvious differences in their qualitative mineral compositions. $Ca(OH)_2$ and CaO are identified as the dominant crystalline phases in the system. Overall, the phase assemblage remains nearly unchanged despite variations in cement content, indicating that cement incorporation does not introduce new major crystalline phases into the SCA matrix. Nevertheless, slight differences can still be observed in the relative intensities of several diffraction peaks. In particular, the diffraction peaks of $Ca(OH)_2$ become more pronounced as the cement content increases to 12%, indicating a stronger crystalline response of $Ca(OH)_2$ in the hydrated SCA system. This trend suggests that moderate cement addition may improve the hydration environment of the CaO-rich matrix, which is consistent with the higher volumetric expansion ratio and expansion pressure observed for Aac60. However, when the cement dosage further increases to 14%, no further enhancement of the $Ca(OH)_2$ diffraction peaks is observed, indicating that excessive cement addition does not continue to improve the crystalline response of the hydrated products. This may be related to the increased water consumption of cement hydration and the denser matrix structure formed at higher cement contents. Therefore, the XRD results are used here to identify the main crystalline phases and compare the relative diffraction features of SCA mixtures with different cement dosages, providing phase-related support for the discussion of the hydration–mechanical behavior.

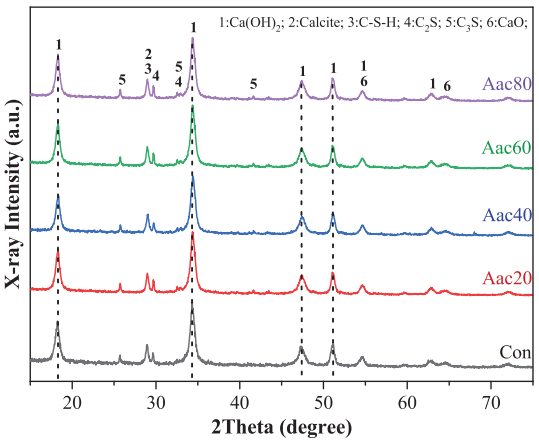

Figure 5 XRD patterns of SCA

3.5.2 SEM

Figure 6 presents typical SEM images of SCA after 1 day of hydration. The SEM observations were used to examine the internal morphology of the hydrated SCA matrix and to compare the morphological evolution of samples with different cement dosages. Compared with Con, the hydrated matrix gradually becomes more continuous as the cement dosage increases. In Aac40 and Aac60, the hydration products appear more continuously distributed within the CaO-rich matrix, indicating that an appropriate increase in cement dosage improves the local continuity of the hydrated structure. This morphological feature is consistent with the higher expansion pressure and volumetric expansion ratio observed for these mixtures.

For Aac80, the matrix exhibits relatively denser hydration-product accumulation compared with Aac40 and Aac60. This denser morphology suggests that excessive cement addition may introduce stronger internal confinement within the hydrated SCA matrix. As a result, the effective macroscopic expansion generated by CaO hydration may be partially restricted, which is consistent with the reduced expansion pressure and volumetric expansion ratio of Aac80 [10].

Overall, the SEM results show that cement dosage affects the morphology of the hydrated SCA matrix. The observed morphological evolution is consistent with the proposed interpretation that moderate cement addition improves matrix continuity and expansion-stress transmission, whereas excessive cement addition may lead to excessive internal confinement and restrict effective expansion.

3.6 Cracking of concrete with SCA

The cracking performance of the SCA mixtures was evaluated using single-hole C30 concrete specimens. Aac40, Aac60, and Aac80 were selected as representative mixtures to investigate the influence of cement content on crack initiation and subsequent crack-width development.

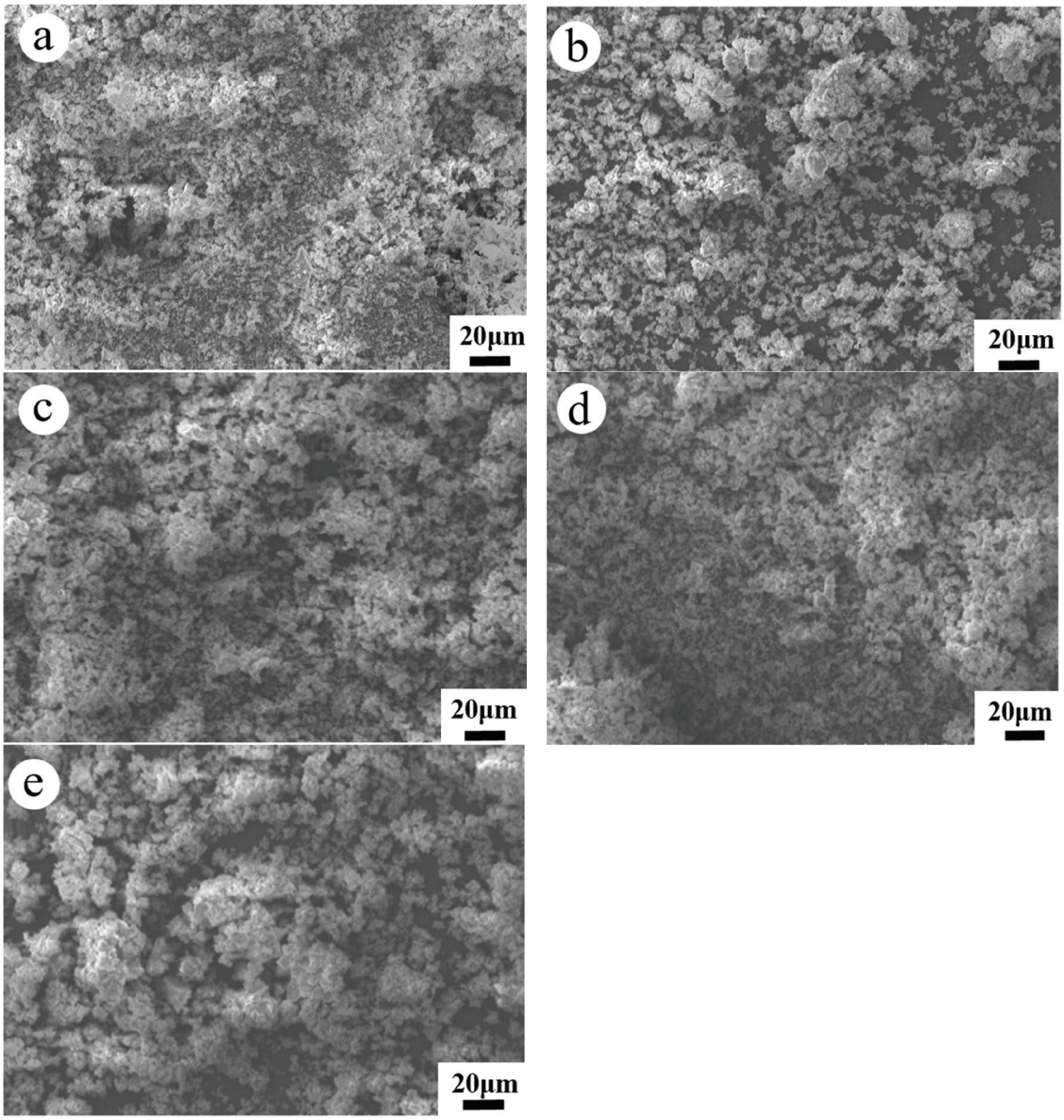

Figure 6 SEM images of SCA: (a) Con; (b) Aac20; (c) Aac40; (d) Aac60; (e) Aac80

The cracking processes are shown in Figure 7, and the corresponding quantitative parameters are summarized in Table 3.

For Aac40, the first visible crack appeared at approximately 60 min, and the specimen reached its final cracking state at approximately 70 min. During this 10 min crack-development period, the crack width increased from approximately 2 mm to 47 mm, corresponding to an average crack-width development rate of 4.50 mm/min. When the cement content increased to 12%, Aac60 initiated cracking at approximately 80 min and reached its final cracking state at approximately 100 min. Its final crack width was approximately 49 mm, and the average crack-width development rate decreased to 2.35 mm/min. Aac80 exhibited the latest crack initiation, at approximately 120 min, and required approximately 40 min to reach its final cracking state at 160 min. Although its final crack width reached approximately 47 mm, its average crack-width development rate was only 1.125 mm/min.

These quantitative results demonstrate that increasing the cement content delays crack initiation and prolongs the subsequent crack-development process. Aac40 provides the earliest crack initiation and fastest crack-width development, whereas Aac60 develops cracks more gradually while exhibiting the highest volumetric expansion ratio. Aac80 shows an excessively delayed and slow cracking response, which may reduce construction efficiency in practical engineering applications.

In addition, the stress generated by SCA expansion must be transferred from the SCA matrix to the surrounding concrete through their contact interface. From a mechanical viewpoint, this interfacial region (often referred to as the interfacial

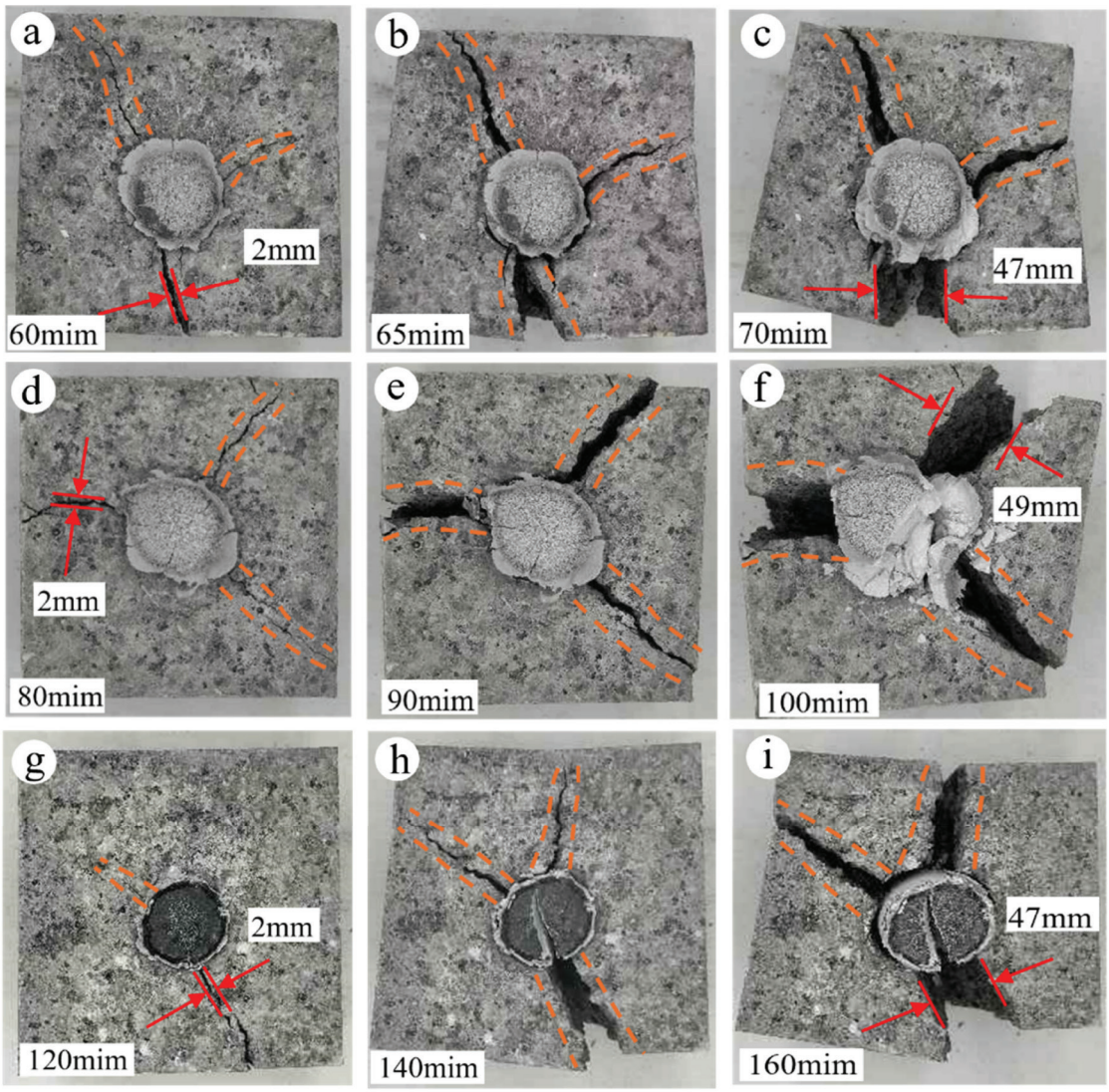

Figure 7 Cracking process of single-hole specimen: (a–c) Cracking process of specimens C30 with the injected Aac40; (d–f) Cracking process of specimens C30 with the injected Aac60; (g–i) Cracking process of specimens C30 with the injected Aac80

Table 3 Cracking data of single-hole specimens with different cement dosages

Group	Crack Initiation Time t_i (min)	Complete Failure Time, t_f (min)	Crack-Development Duration Δt (min)	Final Crack Width w_f (mm)	Average Crack-Width Development Rate v_c (mm/min)
Aac40	60.0 ± 2.0	70.0 ± 2.5	10.0 ± 0.5	47.0 ± 0.8	4.500 ± 0.150
Aac60	80.0 ± 3.0	100.0 ± 4.0	20.0 ± 1.0	49.0 ± 1.0	2.350 ± 0.070
Aac80	120.0 ± 4.0	160.0 ± 6.0	40.0 ± 2.0	47.0 ± 0.9	1.125 ± 0.035

transition zone, ITZ) affects the efficiency of stress transmission. An appropriate cement dosage may improve the continuity and stiffness of the SCA matrix, thereby facilitating stress transfer to the concrete wall. In contrast, excessive cement may delay stress accumulation, leading to postponed crack initiation. From a mechanical perspective, the crack evolution induced by SCA expansion can be regarded as a stress-driven fracture process in concrete. Numerical approaches such as phase-field or damage-based modelling may provide further insight into this mechanism in future studies.

A comparison of the cracking results indicates that the appropriate cement dosage depends on the targeted engineering performance. Aac40, containing 10% cement, exhibits the earliest

crack initiation and the shortest time to complete failure, and is therefore more favorable when rapid cracking efficiency is the primary requirement. In contrast, Aac60, containing 12% cement, develops cracks more gradually but exhibits the highest volumetric expansion ratio. Consequently, 10% cement is preferable for rapid concrete cracking, whereas 12% cement is more suitable for maximizing volumetric expansion and improving reaction controllability. These results demonstrate that no single cement dosage simultaneously optimizes all performance indicators.

3.7 Mechanism summary

Based on the above analysis, the role of cement in the performance of SCA can be qualitatively interpreted through the following two coupled effects:

- **Hydration retarding effect:** The incorporation of cement introduces additional hydration reactions into the CaO-rich SCA system. As cement content increases, part of the mixing water may be consumed by cement hydration, thereby influencing the water availability for CaO hydration and affecting the rate at which expansion develops. This effect provides a qualitative explanation for the observed changes in reaction temperature, expansion pressure, and volumetric expansion ratio with cement dosage.
- **Stress transporting effect:** Cement hydration may contribute to the formation of a relatively continuous hydration-product structure within the SCA matrix, which could influence the transmission of expansion stress generated by CaO hydration. At moderate cement contents, this structural continuity may be beneficial for distributing and transferring expansion stress, whereas excessive cement content may result in a relatively denser matrix and stronger internal confinement, thereby reducing effective expansion.

Overall, these two effects act simultaneously, and the appropriate cement dosage depends on the targeted performance. A cement content of 12% provides the maximum volumetric expansion ratio, whereas 10% results in earlier crack initiation and faster concrete failure. Therefore, a cement dosage range of 10–12% represents a practical compromise between expansion capacity, reaction controllability, and cracking efficiency, rather than a single universally optimal composition.

It should be emphasized that the water-competition effect, structural-confinement effect, and stress-transfer effect proposed in this study are qualitative explanations of the observed macroscopic behavior. Therefore, the mechanism proposed in Figure 8 should be regarded as a conceptual interpretation rather than a quantitatively verified model.

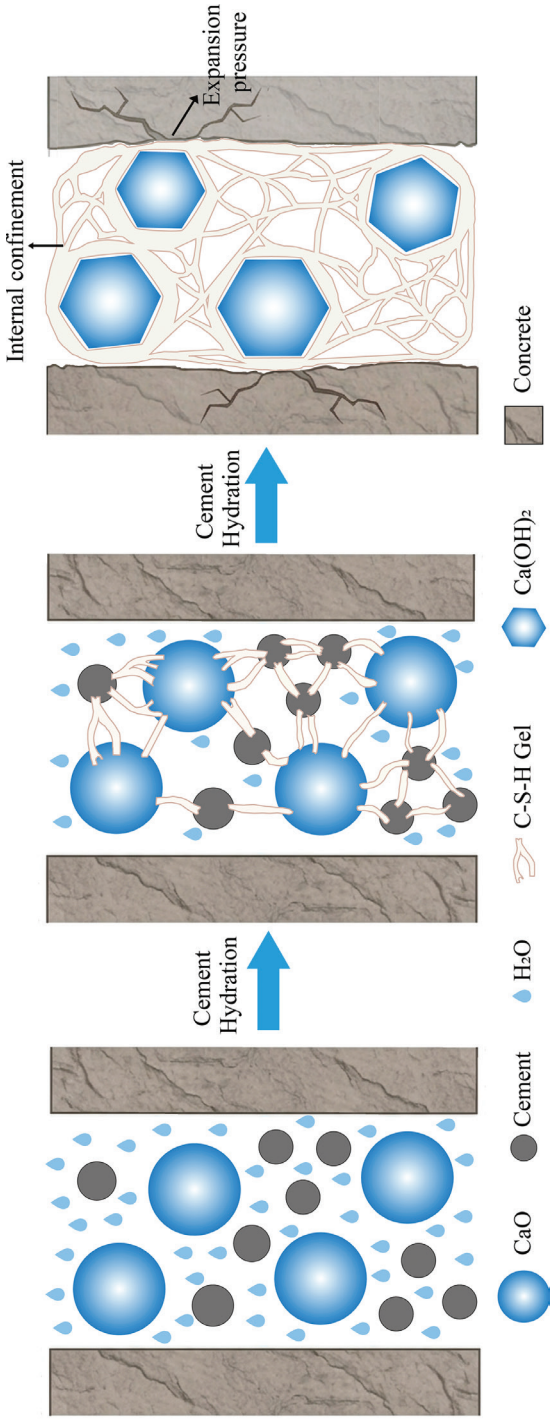

Figure 8 Schematic illustration of the three-stage hydration–mechanical evolution mechanism of cement-modified SCA

4 Conclusions

This study investigated the feasibility of regulating the hydration rate and expansion characteristics of SCA by adjusting cement content. The results suggest that a moderate amount of cement may improve the continuity of the hydrated matrix, thereby facilitating the transmission of expansion stress and producing controllable concrete cracking. In contrast, insufficient cement produced a weakened structural support for hydrated CaO, while excessive cement consumed too much

water and restricted the expansion of SCA. As the cement dosage increases from 6% to 14%, the volume expansion ratio of SCA initially increases and subsequently decreases with the dosage of cement, reaching its maximum at 12%. In terms of reaction rate, an appropriate cement dosage (10–12%) effectively delays the reaction rate without weakening the reaction intensity, thereby providing improved control over the cracking time. However, excessive cement (≥14%) leads to a sharp decline in peak temperature and a smoother temperature evolution curve, indicating an insufficient reaction rate and reduced expansive performance. For crack evolution, SCAs with 10–12% cement content exhibited the most favorable performance, achieving rapid but controllable cracking of concrete specimens. In contrast, insufficient cement resulted in premature cracking, while excessive cement significantly prolonged the initiation and failure times, reducing efficiency. Overall, adjusting cement dosage provides an effective approach to balance expansion efficiency and reaction controllability. A cement dosage range of 10–12% is recommended as a practical application range rather than as a single optimum, with the specific dosage selected according to the required balance between maximum expansion and rapid cracking efficiency.

Acknowledgement

The Analytical and Testing Center of Anhui University of Science and Technology is appreciated for the help in sample analysis.

Funding Statement

This work was supported by the National Natural Science Foundation of China (52227901), Anhui Provincial Key Science and Technology Breakthrough Program Project (202423l10050008), Tongling Science and Technology Plan Project (2023020304).

Author Contributions

Jingshu Shao: Writing—original draft, Methodology, Conceptualization. Peiyuan Chen: Writing—review & editing, Supervision, Resources. Yankun Ma: Visualization, Supervision, Investigation. Aiguo Wang: Visualization, Supervision, Investigation. Weibo Tan: Writing—review & editing. Dingzou Tang: Visualization, Supervision, Investigation. All authors reviewed and approved the final version of the manuscript.

Availability of Data and Materials

Data will be made available on request.

Ethics Approval

Not applicable.

Conflicts of Interest

The authors declare no conflicts of interest.

REFERENCES

[1] Liu H, Li W, Guan W, Zhao H, Yao J, Wen Y. Mechanistic study of a microwave field-controlled static crushing agent for efficient rock breaking. ACS Omega. 2022;7(33):29344–55. doi:10.1021/acsomega.2c03598.
[2] Al-Bakri A, Hefni M. A review of some nonexplosive alternative methods to conventional rock blasting. Open Geosci. 2021;13(1):431–42. doi:10.1515/geo-2020-0245.
[3] Pal Roy P. Emerging trends in drilling and blasting technology: concerns and commitments. Arab J Geosci. 2021;14(7):652. doi:10.1007/s12517-021-06949-z.
[4] Roy PP. Controlled blasting in mines & quarries—a paradigm. Curr Trends Civ Struct Eng. 2019;4(3):1–2. doi:10.33552/ctcse.2019.04.000589.
[5] Laefer DF, Natanzi AS, Zolanvari SMI. Impact of thermal transfer on hydration heat of a soundless chemical demolition agent. Constr Build Mater. 2018;187(6):348–59. doi:10.1016/j.conbuildmat.2018.07.168.
[6] Li S, Li Z, Luo M. Experimental study on reasonable composition and proportion of coal and rock static cracking agent. Blasting. 2018;35:137–53. (In Chinese). doi:10.3963/j.issn.1001-487X.2018.01.022.
[7] Li C, He S, Hou W, Ma D. Experimental study on expansion and cracking properties of static cracking agents in different assembly states. Int J Min Sci Technol. 2022;32(6):1259–72. doi:10.1016/j.ijmst.2022.09.001.
[8] Maneenoi N, Bissen R, Chawchai S. Influence of admixtures on the performance of soundless chemical demolition agents and implications for their utilization. J Sustain Min. 2022;21(2):93–111. doi:10.46873/2300-3960.1350.
[9] Natanzi AS, Laefer DF, Connolly L. Cold and moderate ambient temperatures effects on expansive pressure development in soundless chemical demolition agents. Constr Build Mater. 2016;110(5):117–27. doi:10.1016/j.conbuildmat.2016.02.016.
[10] Hua T, Cao Z, Zhang S, Guo R. Relationship between expansion and strength of cement paste with CaO-based expansive agent. Materials. 2024;17(24):6125. doi:10.3390/ma17246125.
[11] Colombi P, D'Antino T. Analytical assessment of the stress-transfer mechanism in FRCM composites. Compos Struct. 2019;220(5):961–70. doi:10.1016/j.compstruct.2019.03.074.
[12] Yang G, Wang H, Wan-Wendner R, Hu Z, Liu J. Cracking behavior of ultra-high strength mortar with CaO-based expansive agent and superabsorbent polymer. Constr Build Mater. 2022;357(6):129281. doi:10.1016/j.conbuildmat.2022.129281.
[13] Li P, Nie GH. Study on the static cracking agent. J Hubei Univ Natl. 2012;2:159–62. (In Chinese).
[14] AQ 1108-2014. Technical specification of static cracking for underground coal mine. Beijing, China: China Coal Industry Publishing House; 2014.
[15] Li H, Liu JP, Tian Q, Zhang SZ. Hydration kinetics and microscopic analysis of calcium oxide expansion clinker. Appl Mech Mater. 2013;477–478:908–14. doi:10.4028/www.scientific.net/amm.477-478.908.
[16] GB/T 8077-2023. Methods for testing uniformity of concrete admixtures. Beijing, China: Standards Press of China; 2023.
[17] Zhang L, Ding D, Zhao J, Zhou G, Wang Z. Mixture design and mechanical properties of recycled mortar and fully recycled aggregate concrete incorporated with fly ash. Materials. 2022;15(22):8143. doi:10.3390/ma15228143.
[18] Criado YA, Alonso M, Abanades JC. Kinetics of the CaO/$Ca(OH)_2$ hydration/dehydration reaction for thermochemical energy storage applications. Ind Eng Chem Res. 2014;53(32):12594–601. doi:10.1021/ie404246p.
[19] Tong C, Wang L, Wang K, Fu J. Early hydration kinetics of shell ash-based cementitious materials: a low-field nuclear magnetic resonance study. Materials. 2025;18(14):3253. doi:10.3390/ma18143253.
[20] Seo JH, Park SM, Yang BJ, Jang JG. Calcined oyster shell powder as an expansive additive in cement mortar. Materials. 2019;12(8):1322. doi:10.3390/ma12081322.
[21] Guo W, Zou S, Pu S, Zhou Y. Study on the physical and chemical properties of cement-based grout containing coal-fly ash. Materials. 2022;15(24):8804. doi:10.3390/ma15248804.

[22] Hua T, Tang J, Zhu J, Tang H, Liu J. Evolution of the early compressive strength of cement-slag pastes with CaO-based expansive agent. Mater Struct. 2022;55(2):63. doi:10.1617/s11527-021-01809-4.
[23] Cui F, Lei Z, Cheng X, Wu X, Shan P, Lv Z. Mechanism and application of static fracturing technology on deep working face. Adv Mater Sci Eng. 2021;2021(1):5516326. doi:10.1155/2021/5516326.
[24] Alvarez JI, Veiga R, Martínez-Ramírez S, Secco M, Faria P, Maravelaki PN, et al. RILEM TC 277-LHS report: a review on the mechanisms of setting and hardening of lime-based binding systems. Mater Struct. 2021;54(2):63. doi:10.1617/s11527-021-01648-3.
[25] Bogner A, Link J, Baum M, Mahlbacher M, Gil-Diaz T, Lützenkirchen J, et al. Early hydration and microstructure formation of Portland cement paste studied by oscillation rheology, isothermal calorimetry, ^{1}H NMR relaxometry, conductance and SAXS. Cem Concr Res. 2020;130:105977. doi:10.1016/j.cemconres.2020.105977.
[26] De Silva VRS, Ranjith PG, Perera MSA, Wu B, Rathnaweera TD. Investigation of the mechanical, microstructural and mineralogical morphology of soundless cracking demolition agents during the hydration process. Mater Charact. 2017;130:9–24. doi:10.1016/j.matchar.2017.05.004.
[27] Gou J, Li S, Jiang C, Li Z, You G. A study on the influence of gypsum and $Ca(OH)_2$ on the mechanical properties and hydration behavior of multi-component solid waste-based cementitious materials. Materials. 2025;18(9):1964. doi:10.3390/ma18091964.
[28] Li H, Liu J, Wang Y, Tian Q. Simplified chemo-mechanical model of hydration/expansion of calcium-oxide-type expansive agent in cement-based materials. Mag Concr Res. 2020;72(19):1006–15. doi:10.1680/jmacr.18.00450.
[29] Shen P, Lu L, He Y, Wang F, Lu J, Zheng H, et al. Investigation on expansion effect of the expansive agents in ultra-high performance concrete. Cem Concr Compos. 2020;105(6):103425. doi:10.1016/j.cemconcomp.2019.103425.
[30] Huang L, Tang L, Löfgren I, Olsson N, Yang Z. Real-time monitoring the electrical properties of pastes to map the hydration induced microstructure change in cement-based materials. Cem Concr Compos. 2022;132:104639. doi:10.1016/j.cemconcomp.2022.104639.
[31] Taşdoğen AH, Dener M, Benli A, Balun B. Cold-cured alkali-activated slag/Portland cement composites: the role of cement content and alkali dosage on mechanical performance, microstructure, and sulfate durability. Struct Concr. 2026:70466. doi:10.1002/suco.70466.
[32] Rahimi-Aghdam S, Masoero E, Rasoolinejad M, Bažant ZP. Century-long expansion of hydrating cement counteracting concrete shrinkage due to humidity drop from selfdesiccation or external drying. Mater Struct. 2019;52(1):11. doi:10.1617/s11527-018-1307-8.
[33] Bentz DP, Stutzman PE. Curing, hydration, and microstructure of cement paste. ACI Mater J. 2006;103(5):348. doi:10.14359/18157.
[34] Taylor HFW. Cement chemistry. 2nd ed. London, UK: Thomas Telford Publishing; 1997.
[35] Tang S, Wang Y, Geng Z, Xu X, Yu W, Hubao A, et al. Structure, fractality, mechanics and durability of calcium silicate hydrates. Fractal Fract. 2021;5(2):47. doi:10.3390/fractalfract5020047.
[36] Richardson IG. The nature of C-S-H in hardened cements. Cem Concr Res. 1999;29(8):1131–47. doi:10.1016/S0008-8846(99)00168-4.
[37] Ioannidou K, Krakowiak KJ, Bauchy M, Hoover CG, Masoero E, Yip S, et al. Mesoscale texture of cement hydrates. Proc Natl Acad Sci U S A. 2016;113(8):2029–34. doi:10.1073/pnas.1520487113.
[38] Wang J, Gao C, Tang J, Hu Z, Liu J. The multi-scale mechanical properties of calcium-silicate-hydrate. Cem Concr Compos. 2023;140:105097. doi:10.1016/j.cemconcomp.2023.105097.